THE UNIVERSITY of EDINBURGH

Edinburgh Research Explorer

# Survival of Plasmodium falciparum infected Red Blood Cell Aggregates in Elongational Shear Flow

**Citation for published version:**
Jötten, A, Schepp, A, Machon, A, Moll, K, Wahlgren, M, Krüger, T & Westerhausen, C 2024, 'Survival of Plasmodium falciparum infected Red Blood Cell Aggregates in Elongational Shear Flow', *Lab on a Chip*, vol. 24, no. 4, pp. 787-797. https://doi.org/10.1039/D3LC00552F

**Digital Object Identifier (DOI):**
10.1039/D3LC00552F

**Link:**
Link to publication record in Edinburgh Research Explorer

**Document Version:**
Peer reviewed version

**Published In:**
Lab on a Chip

**General rights**
Copyright for the publications made accessible via the Edinburgh Research Explorer is retained by the author(s) and / or other copyright owners and it is a condition of accessing these publications that users recognise and abide by the legal requirements associated with these rights.

**Take down policy**
The University of Edinburgh has made every reasonable effort to ensure that Edinburgh Research Explorer content complies with UK legislation. If you believe that the public display of this file breaches copyright please contact openaccess@ed.ac.uk providing details, and we will remove access to the work immediately and investigate your claim.

OPEN ACCESS

Download date: 27. Jul. 2024

# Survival of *P. falciparum* infected Red Blood Cell Aggregates in Elongational Shear Flow

Anna M. Jötten[1,2], Anabelle Schepp[1], Adam Machon[3], Kirsten Moll[4], Mats Wahlgren[4], Timm Krüger[3], Christoph Westerhausen[1,5,6,*]

[1] Institute of Physics, University of Augsburg, 86159 Augsburg, Germany
[2]Faculty of Physics, Ludwig-Maximilians Universität München, 80539 Munich, Germany
[3]School of Engineering, Institute for Multiscale Thermofluids, University of Edinburgh, Edinburgh EH9 3FB, UK
[4]Department of Microbiology, Tumor and Cell Biology, Karolinska Institutet, 171 77 Stockholm, Sweden
[5]Physiology, Faculty of Medicine, Institute of Theoretical Medicine, University of Augsburg, 86159 Augsburg, Germany
[6]Center for Advanced Analytics and Predicitve Sciences, University of Augsburg, 86159 Augsburg, Germany

*author to whom correspondence should be addressed: christoph.westerhausen@gmail.com

## ABSTRACT

Rosetting, the formation of red blood cell aggregates, is a life-threatening condition in *Malaria tropica* and not yet fully understood. We study rosette stability using a set of microfluidic stenotic channels, with varied narrowing angle and erythrocytes of blood groups 0 and A. We find reduced ability of a rosette to pass a stenosis without disruption, the longer the tapered part of the constriction and the narrower the stenosis is. In general, this ability increases with rosette size and is 5%-15% higher in blood group A. The experimental results are substantiated by equivalent experiments using lectin-induced red blood cell aggregates and a simulation of the underlying protein binding kinetics.

## SIGNIFICANCE STATEMENT

The WHO reported an estimated number of 241 million cases and 627 000 malaria deaths in 2020. The most lethal form is *Malaria tropica* due to erythrocyte aggregates blocking blood flow in capillaries, especially in the brain. It has been shown that the stability of these aggregates under flow is size and blood group dependent. However, it is unclear which physical interaction determines the aggregates fates during passing constrictions. We here show that for different elongational and shear flow application the exposition duration of elongational flow is more relevant than its absolute value, explaining why the aggregates survive the passage of stenoses with an abrupt reduction of the vessel cross section more easily than those with a lower elongational rate.

## INTRODUCTION

The malaria parasite invades red blood cells and causes them to coagulate and form so-called *rosettes*. By rosette formation the binding proteins, which are expressed during parasite development, are covered with uninfected red blood cells. Consequently, rosetting avoids attacks from the immune system (1,2). Rosettes can lead to emboli causing arterial blockage, which results in insufficient oxygen supply of the tissue (3). Blood clots or arterial embolisms that are promoted by rosetting can be fatal for people who suffer from heart diseases (4,5).

The stability of rosettes has been studied since the 1990s, but the binding mechanisms are not fully uncovered (6). Nash et al. used cone-and-plate viscometers (7,8) and micropipettes (7) to unravel that rosettes can form and persist under physiological wall shear stress, which ranges from 0.05 Pa in post-capillary venules to 1 Pa in arteries (8). Wall shear stress of 1 Pa corresponds to a force of $10^{-10}$ N on two cohesive cells (8). Using a viscometer to apply shear stress, rosettes withstand this stress for minutes, while applying the same force using a micropipette disrupts the rosette in seconds (8). Adams et al. studied rosetting in microfluidic flow assays (diameter 800 µm) and found no effect of shear stress between 0.05 Pa and 0.1 Pa (9). These studies, however, did not take the physical confinement in capillaries into account.

To address the open question of rosette stability under different flow conditions, in a previous publication we quantified rosette survival using a set of stenotic channels of different widths of constrictions between 3.5 µm and 14.5 µm (10). We found a correlation of rosette size, channel diameter and blood group regarding the rosettes' stability or ability to deform. Our data revealed that, under physiologically relevant conditions, rosettes in blood group A have a higher frequency and stability compared to blood group O (10). Stability was measured by determining the "critical width" at which only 50% of the rosettes can pass the stenosis undamaged, which was lower for blood group A rosettes. This result is consistent with the observed protection of blood group O individuals against severe malaria (11–14).

We know from other (binding) proteins such as von-Willebrand-Factor (vWF), a key player in blood clotting, that mainly the elongational components of flow drive the activation of vWF (15). The different effects of shear and elongational flow is due to the fact that shear flow contains a rotational component that leads to tumbling instead of stretching (15). However, it is still unclear if in case of rosettes the elongational rate has a similar predominant impact compared to simple shear flow as on vWF. As a working hypothesis, we here assume that this is indeed the case. While in our previous publication (10), the focus was on maximum shear rate values, here we examine the role of the elongational flow.

Following our hypothesis, we refined the set of stenoses, keeping the constriction width close to the above-mentioned critical width of approx. 5 µm, and varying the elongational length or the steepness of the narrowing part of the stenosis. This approach allows us to separate the influence of the shear rate perpendicular to the flow and the elongation rate along the direction of the flow. We continue studying rosetting in blood groups O and A, and classifying the rosettes by size. Additionally, we use lectin-induced red blood cell aggregates as a model system and perform the same experiments on those. We complete the study with a simulation of the underlying protein binding kinetics, based on Kramers' theory and a simple Monte Carlo simulation of a two-state-model (bound and unbound state) that complements the experimental results.

METHODS

**Sample Preparation**

*i)* *Plasmodium falciparum* infected rosettes

We cultivated the *P. falciparum* laboratory strain S1.2 (16) according to standard methods and synchronized it using 5% sorbitol (16). Prior to experiments, we identified the stage of the parasite by staining of fresh culture with Acridine Orange and subsequent microscope analysis. We enriched the parasitized red blood cells (pRBCs) around 32–38 h *post invasion* by magnetically activated cell sorting (MACS, Miltenyi Biotec), as described earlier (16), resulting in 70–90% parasitemia. We resuspended the enriched pRBCs with unparasitized RBCs in MCMS, malaria culture medium containing 10% filtered human serum, to reach a final parasitemia of 20% and a hematocrit of 1%. The added unparasitized RBCs were of blood group O and A for the measurements in the respective blood groups, while blood group O RBCs were used for cultivation of the parasite. After two hours of incubation, rosettes have formed. A rosette is by definition composed of one infected and at least two unparasitized cells. Other forms of aggregation like auto-agglutination between infected cells and rosettes with more than one infected cell can occur, but these aggregates form rarely, as reviewed by optical controls.

*ii)* Lectin-induced aggregation

The lectin Wheat Germ Agglutinin (WGA) is used, from here on referred to as lectin. A suspension of RBCs, hematocrit H = 2 %, in 500 µl PBS and a lectin concentration of c = 4 µg/ml, is prepared. After 10 minutes at room temperature to allow for aggregation, the suspension is washed three times. The washing step involves centrifugation at 3000 $min^{-1}$ for 3 minutes, removal of supernatant, and resuspensation in 500 µl PBS.

**Microchannel Design and Measurement Setup**

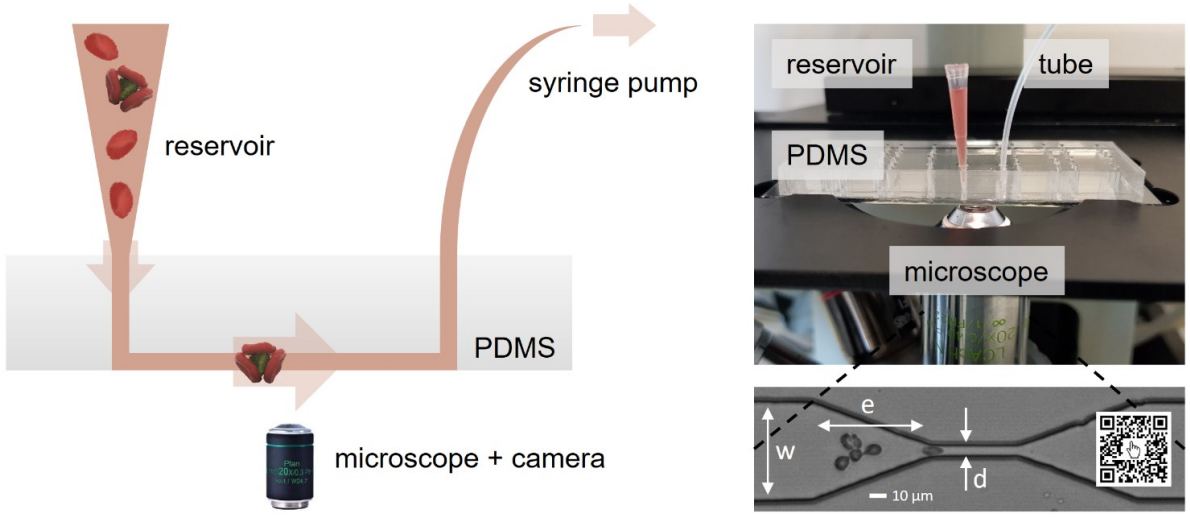


*Figure 1 Microfluidic setup consisting of a microfluidic channel in PDMS on a glass slide, a pipette tip as sample reservoir at the channel inlet and a PTFE tube at the channel outlet connected to a syringe pump. The channel width w is gradually reduced to the stenosis diameter d over the length e. Micrographs are recorded using an inverted microscope.*

The microchannel consisted of a polydimethylsiloxane (PDMS) single layer fabricated by standard soft lithography (17), which was bonded on a glass slide by plasma activation (Fig. 1). Generally, all channels in our set were 7 mm long, 8 µm in depth and 50 µm in width. The

central part of interest comprised a single stenosis in which the channel width was reduced from w = 50 µm to one of the two chosen values d = 5 µm and d = 7 µm, respectively, if not mentioned otherwise. Four differently steep stenoses were combined with each constriction width (Figure 2). The length of the stenosis designated as "standard elongation" complies with a narrowing angle of 20° or an elongational length $e$ of $e = e_{std} = 55\mu\mathrm{m}$. One steeper angle, resulting in "one fifth elongation", $e = 0.2e_{std}$, and two smaller angles complying with "double elongation" ($e = 2e_{std}$) and "triple elongation" ($e = 3e_{std}$) were chosen.

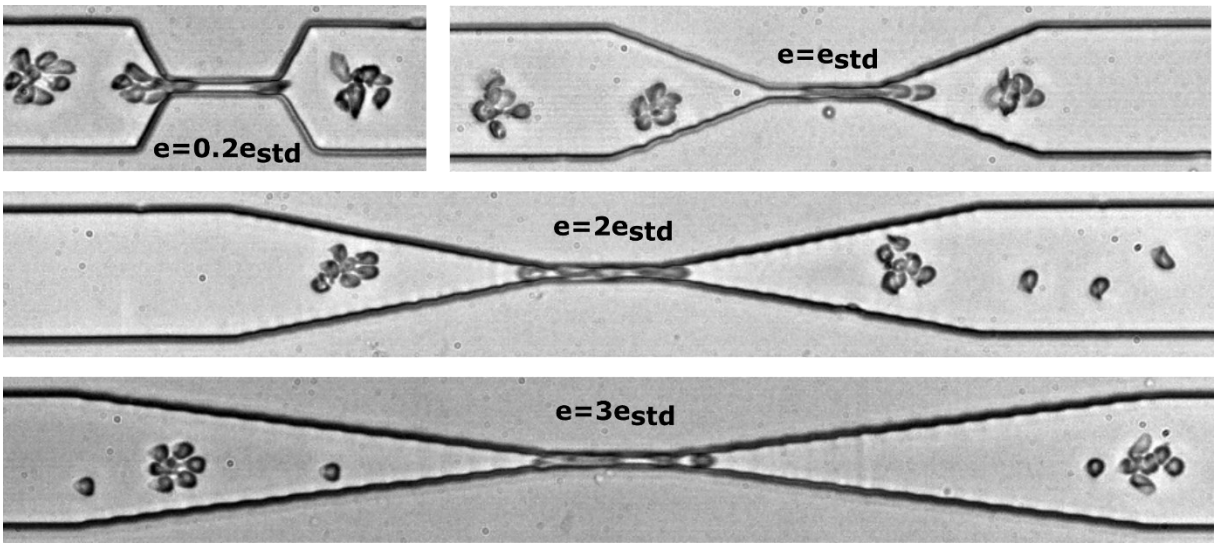


*Figure 2 Set of different stenoses used in the experiments. All channels are constantly 8 µm deep and initially 50 µm wide, narrowing to a stenosis of 5 µm width (or 7 µm, not shown) over a varied elongational length of $e = 0.2e_{std}; e_{std}; 2e_{std}$ and $3e_{std}$ with $e_{std} = 55\mu m$. Top row images are cropped, lower two images are in original size (704x66 µm²).*

The complete setup as depicted in Figure 1 consisted of the microchannel, a pipette tip serving as the cell suspension reservoir and a syringe pump (Harvard PHD2000, Harvard Apparatus). A Hamilton Gastight Syringe (Hamilton Bonaduz AG) containing phosphate-buffered saline (PBS, pH = 7.4) was connected to the microchannel via a polyfluoroethylene (PTFE) tube (inner diameter 0.38 mm). The pump was operated in reverse mode to provide controlled flow by drawing the suspension from the reservoir through the microfluidic channel resulting in flow rates Q in the range of 15 µl/h < Q < 25 µl/h. We observed the cells using the 20x objective (Nikon Plan ELWD CFN 20x 0.40 160/1.2 Ph2 DM Microscope Objective Phase Contrast) of an inverted microscope (Nikon Diaphot 300) in brightfield-mode equipped with a high speed video camera (FASTCAM Mini UX50 type 160K-M-16G, Photron). The videos were recorded with the software Photron Fastcam Viewer PFV from Photron at 2000 frames per second, 1280x120 pixel resolution, and 1/32000 seconds exposure, resulting in a maximum total of 74531 frames or 37 seconds in real time covering an area of 704x66 µm².

**SURF tracing and categorizing**

For analysis we developed the customized software SURF (SUrvival of Rosettes in Flow), a MATLAB© based tracking algorithm to follow and analyze rosettes along a microfluidic channel. The functionality was published earlier (10,18).

**Categorize by size.** The "size" of the rosettes $A_{ros}$ denotes here the cross-sectional area as optically appearing in the micrographs. The rosettes' radius $r_{ros}$

$$r_{\mathrm{ros}} = \sqrt{A_{\mathrm{ros}}/\pi} \tag{1}$$

is the radius of the equivalent circle with area $A_{ros}$, respectively. For further analysis, these traces are categorized according to the initial rosette size $A_{ros}$ being normalized to the area of a single red blood cell $A_{RBC}$. The histogram edges used are set to 1.11, 2.22, 3.33, 4.44, 5.56, 7.78 and 30 $A_{RBC}$, and classified into classes 1–6. Cell aggregates in class 1 consist often only of two cells. A rosette is by definition composed of one infected and at least two unparasitized cells, therefore only cell aggregates from classes 2–6 are taken into account in the results section.

| | single RBC | rosette class 1 | rosette class 2 | rosette class 3 | rosette class 4 | rosette class 5 | rosette class 6 |
|---|---|---|---|---|---|---|---|
| area | $A_{RBC}$ | $1.11A_{RBC} < A_{ros} < 2.22A_{RBC}$ | $2.22A_{RBC} < A_{ros} < 3.33A_{RBC}$ | $3.33A_{RBC} < A_{ros} < 4.44A_{RBC}$ | $4.44A_{RBC} < A_{ros} < 5.56A_{RBC}$ | $5.56A_{RBC} < A_{ros} < 7.78A_{RBC}$ | $7.78A_{RBC} < A_{ros} < 30A_{RBC}$ |
| | 1 cell | 1-2 cells | 2-3 cells | 4-5 cells | 6-7 cells | 7-10 cells | 11-20 cells |

*Table 1 Classification of rosettes in classes 1-6 respective to their cross-sectional area, compare previous publication* (10)

**Categorize by fate.** If a rosette is being traced along the channel, main events such as rupture and total disruption are identified and listed (compare (10)). Following a rosette squeezing through a stenosis, one of three possible scenarios can be observed: (i) a rosette can either pass undamaged, or (ii) damaged, i.e., suffering from a certain cell loss but still being large enough to be considered a rosette, or (iii) become totally disrupted, i.e. losing so many cells that the remaining aggregate falls into class 1.

## Modelling break-up by shear forces

Since cell adhesion is mediated by proteins (19,20), a theoretical model of such proteins is developed and described here. First, in general about $N_{proteins} = 10^5$ proteins are involved in the binding of pRBC to the other RBC in a rosette (21). Secondly, these proteins are clustered in so called knobs. As a consequence in our model we assume binding spots (consisting of a larger number of protein-protein-bonds) that can either be in the state “bound” (1) or “detached” (0), and within a time period Δt with a probability P, which is the product of the binding or unbinding rate k and the time span Δt. Thus, for a single binding spot, a simple random experiment can be performed by creating a (pseudo) random number z ∈ [0, 1) that is compared with the probability P. If one simulates the behavior of several such binding spots in parallel, the model can be applied to the disintegration or cohesion of entire cell aggregates. In concrete terms, the simulation is implemented as follows: First, the intrinsic tie-off and tie-on rates $k_{on,0}$ and $k_{off,0}$ are determined. The initial equilibrium constant K

$$K = \frac{k_{on,0}}{k_{on,0} + k_{off,0}} \tag{2}$$

determines how many of the $N_{total}$ binding spots are in the bound state at the beginning. This means

$$N_{on,0} = KN_{total}. \tag{3}$$

Assuming a sufficiently high equilibration time prior to reaching the stenosis region, we set the number of bound binding spots to the equilibrium value predicted by *K*. In the example in Figure 7 $N_{on,0} = \frac{1000}{1200} * 200 = \frac{1000}{6} \approx 166$ binding spots of the $N_{total} = 200$ bindind spots are in the bound state "1", the remaining $N_{total} - N_{on,0} = 34$ in the unbound state "0". In each simulation step, a random experiment now takes place for each binding spot. For this purpose, the rates $k_{on}$and $k_{off}$ must be known. In general, the rate according to Kramers (20,22,23)

depends on the force F acting on the binding spot and the distance between initial and transition state x,

$$k_{off} = k_{off,0} e^{\frac{Fx}{k_B T}}. \tag{4}$$

The force F acting here is a combination of drag force and compressional forces, which is a function of the square of the velocity following the argumentation of Armistead et al. (24). Thus, to reproduce the experiment of the passage of a stenosis, the velocity v(t) must be included into the calculation of the rate. The force per binding spot can be estimated by the number of proteins accumulated in knobs on the surface of an infected red blood cell. The surface has approximately 1000 such knobs. The ratio $\frac{F}{N_{total}}$ is given by the product of a constant c´ and the square of the velocity.

$$\frac{F}{N_{total}} = c' v^2 \tag{5}$$

Moreover, assuming a constant distance x, meaning protein stretching, between the initial state and the transition state we summarize c´ and the constant $x/k_B T$ in the constant c.

$$\begin{aligned} k_{on} &= k_{on,0} e^{-cv^2} \\ k_{off} &= k_{off,0} e^{cv^2} \end{aligned} \tag{6}$$

Furthermore, the force is distributed exclusively among the bound binding spots. Thus, the force must be corrected by the factor $\frac{N_{total}}{N_{on}}$.

$$\begin{aligned} k_{on} &= k_{on,0} e^{\frac{-N_{total}}{N_{on}} cv^2} \\ k_{off} &= k_{off,0} e^{\frac{N_{total}}{N_{on}} cv^2} \end{aligned} \tag{7}$$

The initial conditions are set by the fixed, but arbitrarily chosen, parameters $k_{on,0} = 1000$ and $k_{off,0} = 200$. To estimate the value of the parameter $c$ from the drag force we in the first step assume that the overall force pulling at the rosette is distributed over all involved proteins $N_{proteins} = 10^5$. This results in:

$$cv^2 = \frac{Fx}{N_{proteins} k_B T} = \frac{\frac{1}{2} \rho C_W r^2 \pi v^2 x}{N_{proteins} k_B T} \approx 130 v^2 \tag{8}$$

The drag force is expressed by the fluid density $\rho = 1000 \frac{kg}{m^3}$, the drag coefficient $C_W = \frac{24}{Re}$,the rosette radius $r$ and the flow velocity $v$. A rosette radius of r = 12 µm is chosen here to roughly estimate $c$. For other rosette sizes correspondingly different values between $c = 90$ for $r = 10\mu m$ and $c = 200$ for $r = 15\mu m$ have been chosen. In addition, the value depends on the choice of the characteristic bond length x = 1 nm and the Reynolds number, which is kept constant here at Re = 0.1 as a further simplification. To reproduce the velocity course of a stenosis, in each time step Δt the travelled distance Δx is calculated from the current velocity. Then, at the new position the new velocity is calculated over the current channel width d as a function of elongation length e and length of the narrowest part of the stenosis l.

If at least one of the simulated $N_{total}$ binding spots is still bound after passage of the location of the stenosis in the simulation, it has "survived", and the equilibrium $N_{on,0}$, which prevailed before the stenosis, can be restored. If, at any time, all binding spots are detached simultaneously, the aggregate is considered disintegrated, and rebinding is no longer possible. Such an aggregate has "not survived". For multiple runs $r$ of the simulation with a group of $N_{total}$ binding spots, it is possible to determine a survival rate $s_{sim}$ based on the number of runs in which the stenosis was survived $r(N_{on,end} > 1)$, and the total number of runs $r_{total}$ .

$$s_{sim} = \frac{r(N_{on,end} > 1)}{r_{total}} \tag{9}$$

RESULTS AND DISCUSSION

**State of the Rosettes after passing a stenosis**

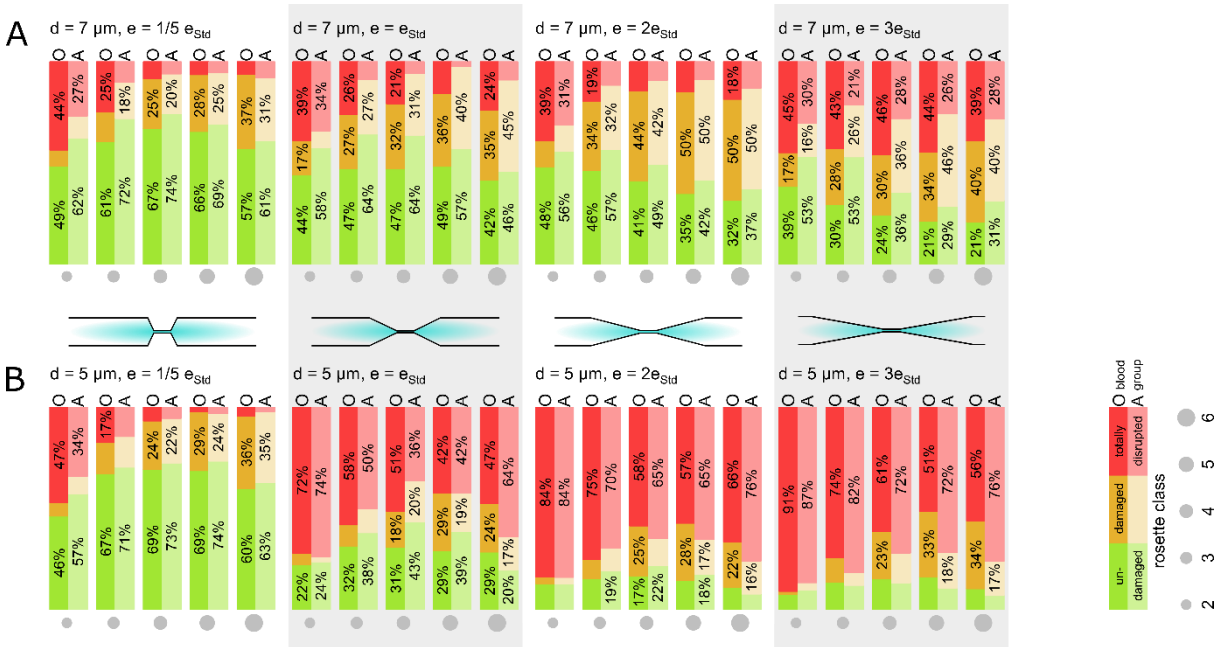


*Figure 3 The state of a rosette after passing a stenosis is either „undamaged" (green), „damaged" (yellow) or „totally disrupted" (red). The flow rate Q was in the range of 15 µl/h < Q < 25 µl/h. The bar charts show the distribution on those three states for stenoses of two different widths A) d = 7 µm, B) d = 5 µm and four different elongational lengths. Besides the standard elongation measuring $e_{Std} = 55$ µm, there is one shorter version with $e = 0.2e_{Std}$ and two longer versions with $e = 2e_{Std}$ and $e = 3e_{Std}$. The area of the grey circles represents the size of a rosette of the respective rosette class* (10). *Results in blood groups A and O are labelled A and O, respectively.*

The colored bars in Figure 3 A and B depict the distribution of rosette states for blood group 0 and A directly after passing a stenosis of width 7 µm and 5 µm, respectively. From left to right, the elongation length is varied from 0.2 $e_{Std}$ to 3 $e_{Std}$. These states are denoted (i) undamaged (green), (ii) damaged (orange) and (iii) totally disrupted (red). Both figures summarize the results of 500–1500 traced rosettes being classified into categories 2–6. The experiments result in 95% confidence intervals of 5% on average.

We confirm two effects that we have reported earlier (10). Firstly, the percentage of totally disrupted rosettes is higher for smaller rosettes than for larger ones (class 2-5). Secondly, more rosettes are disrupted passing the narrower stenosis with d = 5 µm than the one with d = 7 µm. Beyond these observations, we found a significant impact of the elongational length that has not been investigated previously. The longer the stenosis, the fewer rosettes pass without damage. Comparing the survival rate, which comprises the undamaged and damaged

rates (green and orange bars), between both diameters d = 5 µm and d = 7 µm at each elongational length individually, we find almost equal results for the shortest stenosis ($e = 0.2e_{Std}$), while longer stenoses lead to significantly lower survival rates for the d = 5 µm stenosis. The impact of the length of the stenosis is remarkably smaller for the wider stenosis with d = 7 µm: for all values of e, the survival rate ranges from 75% to 90%. For the narrower stenosis with d = 5 µm, however, the results cover a much wider range from 30% to 85%. The longer the stenosis, the fewer rosettes remain undamaged. An abrupt constriction, accompanied with a higher elongation rate, seems to affect a rosette less than the continuous extension when passing a longer stenosis. This is in contradiction to our initial working hypothesis. The leading cause, besides the immediate lengthening of the rosette, could be the longer exposure time to higher shear and elongational stresses in longer stenoses.

When comparing rosettes with different sizes (between class 3 and 6), we find a decreasing percentage of undamaged rosettes. At the same time, the percentage of damaged rosettes increases to such an extent that the total survival rate slightly increases with rosette size. The number of totally disrupted rosettes increases with rosette size between class 2 and 5, while class 6 rosettes behave contrary to the systematic. We relate this to their different nature, considering the large number of 11-20 RBCs in class 6 rosettes, most likely involving not only one central pRBC but two or more pRBCs each. Comparing blood groups O and A, the survival rate is 5-15% higher in blood group A. Both the size and blood group effects are in line with earlier works (10). Exceptions occurred at d = 5 µm with $e = 2e_{Std}$ and $e = 3e_{Std}$, where the survival rate of blood group O rosettes exceeds those of blood group A.

**Transition Length**

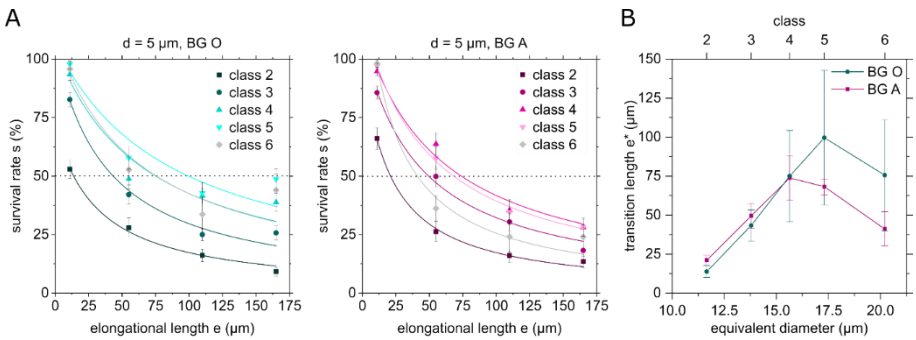


*Figure 4 Impact of the elongation in a stenosis on the disruption of rosettes. A) Survival rate of rosettes of rosette classes 2–6 in blood group O (left) and A (right) as a function of elongational length when passing stenoses of different lengths and fixed width of d = 5 µm fitted using equation 10. Error bars are 95% confidence intervals. B) Transition length e*, which results from fits in A, as a function of the rosette size. The transition length e* is defined as the critical length beyond which the survival rate drops below 50%.*

Plotting the survival rate as a function of the elongational length *e*, reveals a hyperbolical relation. The phenomenological fit function *s(c,e)* describes the survival rate *s* for rosette class *c* as a function of the elongational length *e* using the descriptive parameters *p* and *q*:

$$s(c,e) = \frac{1}{p + qe} \tag{10}$$

From the fit function, the length e* that corresponds to a survival rate of 50% can be calculated:

$$s(c, e) = 0.5 \tag{11}$$

The curves in Figure 4 correlate with values of $p \approx 1$ and $q \approx 0.02\ \mu\mathrm{m}^{-1}$. Accordingly, the transition length falls with e* ≈ 50 µm into the experimental range and increases with aggregate size, see Figure 4B. The difference between blood groups is not significant.

Looking at wider stenoses with d = 7 µm, the influence of the elongational length is negligible. As the respective curves never drop below s = 50%, we do not explicitly show them or extract a transition length here.

## Experimental Model: Lectin-induced aggregation

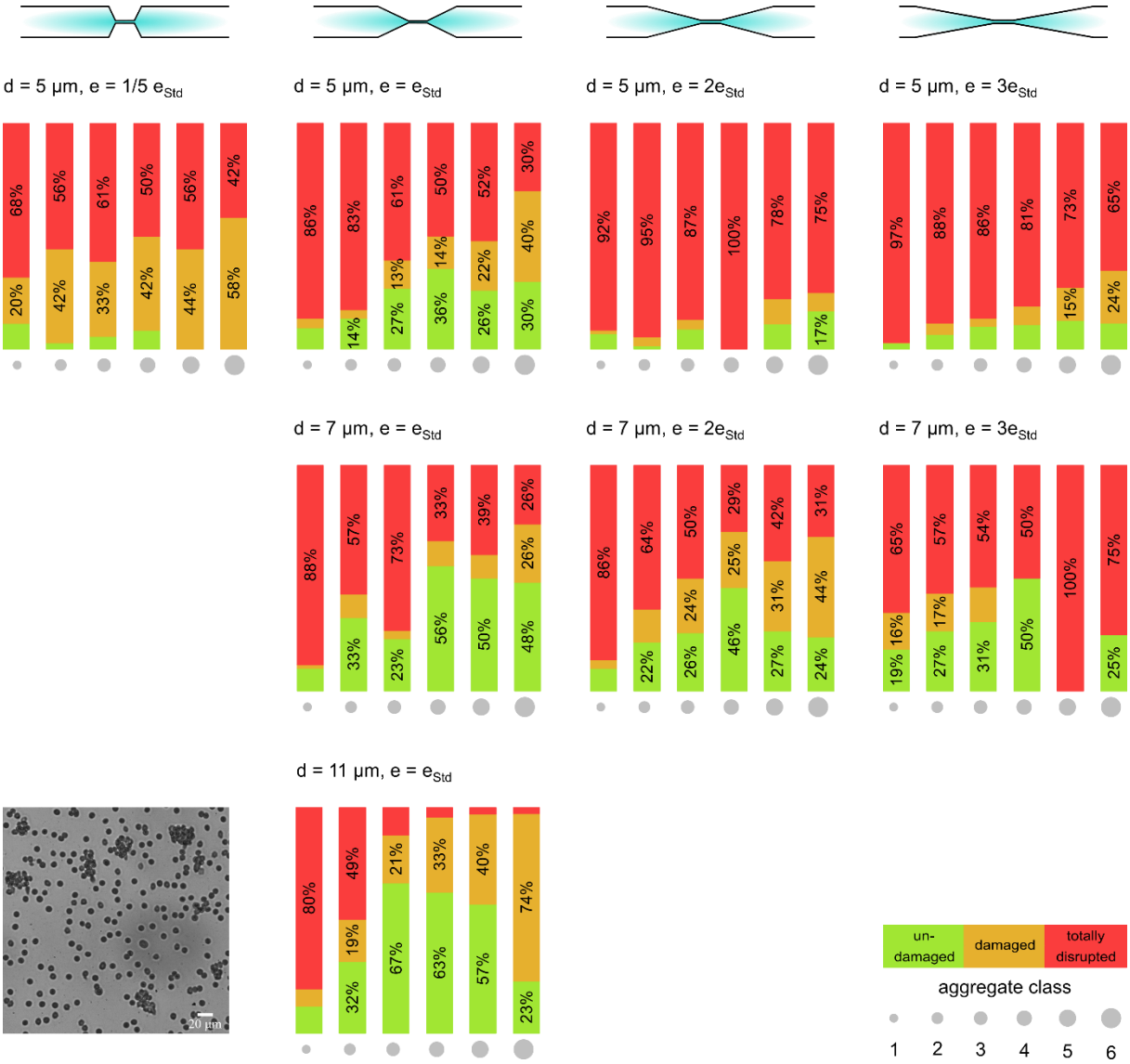


*Figure 5 States of lectin-induced aggregates after passing different stenoses at flow rates Q in the range of 7 µl/h < Q < 15 µl/h.. The state of a lectin-induced aggregate after passage of a stenosis is either "undamaged" (green), "damaged" (yellow) or "totally disrupted" (red). The distribution among these three states for stenoses of three different widths (d = 11 µm, d = 7 µm, and d = 5 µm) and different elongational lengths (e = 0.2$e_{std}$, $e_{std}$, 2$e_{std}$ and 3$e_{std}$), standard elongation length eStd = 55 µm, is shown. The area of the gray circles at the bottom corresponds in each case to the size of the aggregates in the relevant class 1–6. Inset: Lectin-induced aggregation of red blood cells.*

To compare rosetting to other types of binding and to evaluate the stability of rosettes further, the same flow experiments are performed with lectin-induced aggregates as a model system. Lectins bind to membrane receptors of erythrocytes and induce clumping. In contrast to rosettes, where an infected cell forms the center from which adhesion molecules protrude, in lectin-induced aggregation all cells behave equally regarding cell-cell adhesion. However, the interactions resemble one another (25) and we optimized the lectin concentration and protocol to produce aggregates, which are convincingly similar to rosettes in shape and size distribution (see inset Figure 5). We do not focus on the effect of the blood group here, but all lectin experiments shown here were performed with blood group A. Classification by size follows the lines established for malaria rosettes. Since there is no reason to ignore class 1 in this case, all aggregates of classes 1–6 are considered here.

The influence of the elongation length can be seen in Figure 5 from left to right. If the elongation length is increased at a stenosis width of d = 5 µm, a strong decrease of the survival rates can be seen (see Figure 5 top row). At the steepest elongation of $e = 0.2e_{Std}$, almost 70% of the small aggregates are completely disrupted, whereas only a fraction of about 10% passes the stenosis unharmed. If the aggregates increase in size, up to 50% survive the stenosis, but significantly more are damaged in the process, until there are no undamaged aggregates left in classes 5 and 6. Increasing the stenosis length, the trend continues for the larger aggregates to pass the stenosis in significantly greater numbers. About 15% of the aggregates survive the standard length in class 1 and already 70% in class 6, with about 10-35% of the aggregates remaining completely intact. If the elongation is increased to two or three times the standard length, more than 90% of the aggregates in class 1 are already disintegrated. This value decreases continuously with increasing aggregate size until, in class 6, 75% or 65% of the aggregates remain undamaged. The rate of undamaged aggregates is consistently similar at about 10%. Particularly with triple elongation, the proportion of damaged aggregates increases significantly from 5% to 25%.

A similar behavior can be seen for the channels with a stenosis width of d = 7 µm (see Figure 5 second row). For the standard elongation and two- and threefold lengths, the undamaged rate increases from about 10% to a local maximum at class 4 with about 50%. In the standard case $e = e_{std}$, this level of around 50% undamaged rosettes remains largely unchanged between classes 4, 5 and 6, but in the longer stenosis it falls back to 25% for classes 5 and 6. The rate of damaged aggregates increases noticeably with aggregate size, most prominent in the results for d=7µm, $e = 2e_{std}$. The triple elongation results show almost no damaged aggreates, which is probably due to the sparse data available. In the first three classes, approx. 15% of 15-40 aggregates are damaged; for larger aggregates, the counts are only 2-4; consequently, the distribution is not statistically significant. For all other measurements, the trajectories of 50-500 aggregates are included per measuring point, i.e. per class and channel shape. In Figure 6 the corresponding 95% confidence intervals are plotted.

Next, we discuss Figure 5, second column, to focus on different widths (d = 5 µm, d = 7 µm and d = 11 µm) at fixed elongation $e = e_{Std}$. For d = 11 µm, the fraction of undamaged aggregates (green) is maximal in classes 3 and 4, up to 67%, exceeding the fraction in class 1 by more than five times. If the aggregate size continues to increase, the probability of undamaged aggregates decreases. The proportion of damaged aggregates (yellow), on the other hand, increases with aggregate size from 5% to up to 74%. At a stenosis width of 11 µm, it can be clearly seen that the narrowing of the cross-section is not sufficient to affect the large aggregates. Only 3% of the largest aggregates are totally disrupted.

Overall, the same trends that occur for rosettes can be found here. The narrower and the longer the stenosis, the more aggregates are damaged or disintegrated. Having a closer look at the survival quantities in Figure 3 for rosettes and Figure 5 for lectin-induced aggregates, as summarized in Table 2, lectin-induced aggregates appear to be less stable than rosettes. Looking at the average survival for all size classes, for d = 7 µm, for example, only about 30% of rosettes are totally disrupted, but about 60% of lectin-induced aggregates are. The situation is even more pronounced for d = 5 µm. Here, only 10–20% of the lectin-induced aggregates remain undamaged, while approx. 70-90% are totally disrupted. For rosettes, the same conditions result in 20–30% undamaged and only about 70% totally disrupted.

| Survival rate | | | | | Undamaged rate | | | | |
|---|---|---|---|---|---|---|---|---|---|
| **5 µm** | 0.2 EL | EL | 2 EL | 3 EL | **5 µm** | 0.2 EL | EL | 2 EL | 3 EL |
| BG O | 81% | 45% | 36% | 35% | BG O | 62% | 29% | 15% | 14% |
| BG A | 90% | 50% | 30% | 23% | BG A | 69% | 34% | 17% | 11% |
| Lectin | 41% | 27% | 9% | 8% | Lectin | 6% | 16% | 6% | 5% |

| Survival rate | | | | | Undamaged rate | | | | |
|---|---|---|---|---|---|---|---|---|---|
| **7 µm** | 0.2 EL | EL | 2 EL | 3 EL | **7 µm** | 0.2 EL | EL | 2 EL | 3 EL |
| BG O | 81% | 75% | 79% | 56% | BG O | 61% | 46% | 42% | 29% |
| BG A | 90% | 91% | 87% | 74% | BG A | 69% | 58% | 48% | 41% |
| Lectin | | 30% | 25% | 38% | Lectin | | 23% | 15% | 23% |

*Table 2 Survival and undamaged rates independent of the cell aggregate size (weighted average over all classes) for blood groups A and O (compare Figure 3) and Lectin-induced aggregates (compare Figure 5).*

To further compare the stability of rosettes and Lectin-induced aggregates, we repeat the analysis from Figure 4 and evaluate the survival rate *s* as a function of elongation length for the Lectin-induced aggregates (Figure 6). As already observed for rosettes, the curves for the narrower stenosis with d = 5 µm drop systematically, whereas the level at d = 7 µm does not seem to depend significantly on the elongation length. For the experimentally obtained survival rate of rosettes, equation 1 allowed us to determine the transition length $e*$ at a survival rate of 50%. Here, in Figure 6A, the values barely exceed the 50% mark. Thus, the fitted transition lengths are very short with $e* < 10$ µm compared to the transition lengths e*=50-100 µm we found for rosettes, compare Figure 4.

Rosettes and lectin-induced aggregates thus behave qualitatively similarly. Cell-cell binding, which is a specific ligand-receptor binding in both cases, seems to be significantly more stable for *PfEMP1*. Thus, lectin-induced aggregates are suitable as a qualitative model that captures the general trends of aggregate break-up in stenoses. However, since lectin-induced bonds are weaker and fewer than bonds in malaria aggregates, the quantitative behaviors are different.

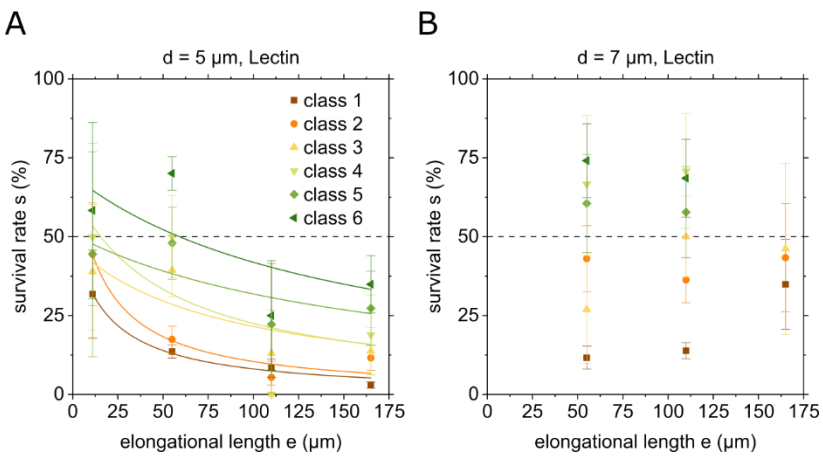


*Figure 6 Elongation-induced disassembly of Lectin-induced aggregates. Survival rate s for aggregates of classes 1–6 as a function of elongation length upon passage of single stenoses of four different lengths from e = 0.2 $e_{Std}$ = 11 µm to e = 3$e_{Std}$ = 165 µm at fixed width A) d = 5 µm and B) d = 7 µm. The error bars represent the 95% confidence intervals. A) Resulting transition lengths e*: e*(class 1) = 0.1 µm, e*(class 2) = 8 µm, e*(class 3) = -4 µm, e*(class 4) = 15 µm, e*(class 5) = 3 µm, e*(class 6) = 59 µm.*

For both rosettes and other cell aggregates, the shape of the stenosis strongly determines the ability of the cell aggregate to pass through it. Firstly, the diameter *d* is relevant. If *d* is narrow

enough to impair the rosettes or aggregates noticeably, the length e of the narrowing part plays an important role. An abrupt constriction is less fatal than the continuous narrowing over a longer distance. During passing such a constriction a rosette can be deformed by compressing the entire rosette and the rearrangement of the cells. How much cells are moved relatively to each other, and whether the bonds can persist during the process, is most likely dependent on the exposure time inside the stenosis and therefore its length. To further elucidate the role of the elongation length, we designed a simple simulation of the protein binding kinetics. As described in the methods section this simulation does not include a molecular picture or account for geometric factors like the position of the remaining binding spots. However, it sufficiently well illustrates how number of binding spots between aggregated RBCs and the stenosis geometry result in characteristic survival rates.

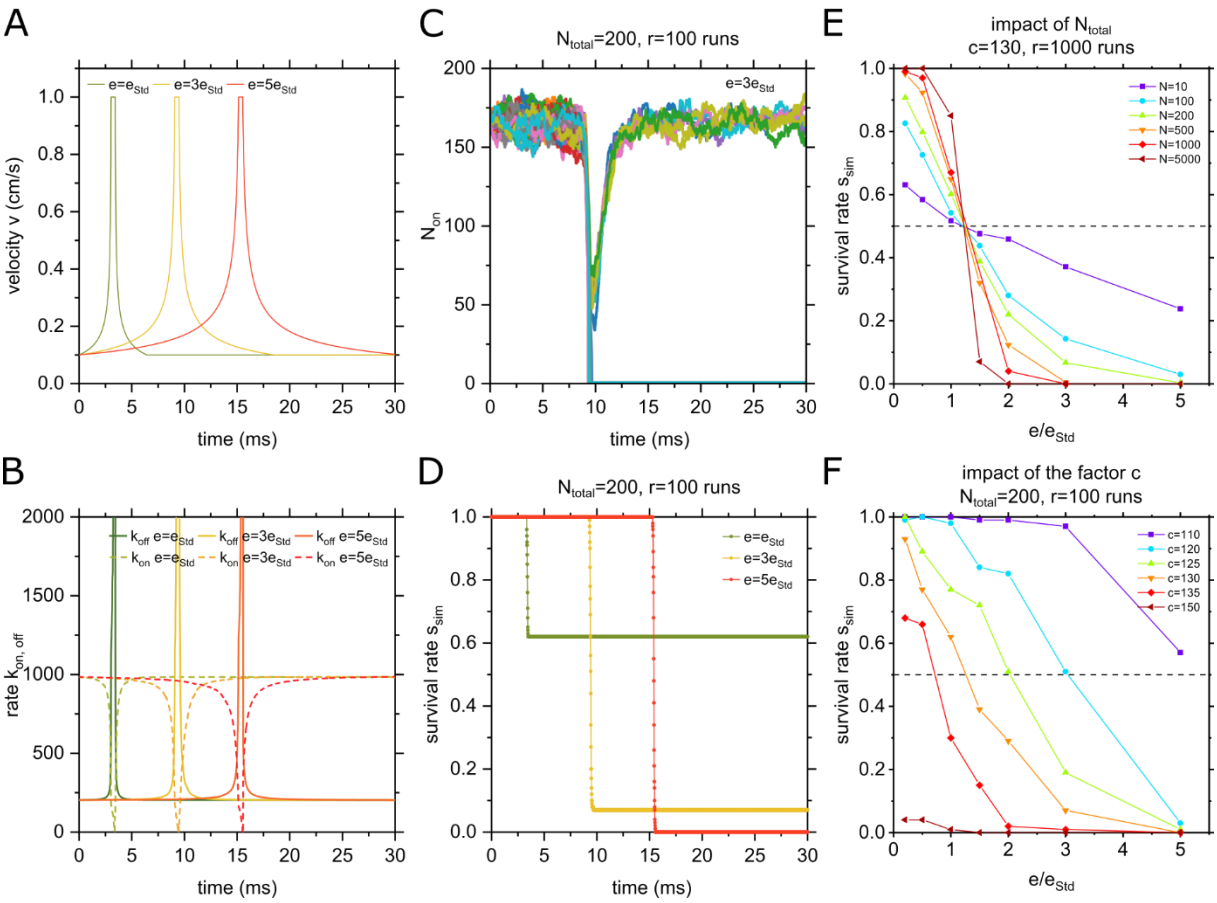


*Figure 7 Simulation of the binding kinetics. A) velocity and B) tie-on and tie-off rates for three different elongational lengths with number $N_{total}$ = 200 and c = 130. C) Simulation result $N_{on}(t)$ for $N_{total}$ = 200, e = $3e_{Std}$ and 100 runs and D) survival rate as a function of time for e = $e_{Std}$, e = $3e_{Std}$ and e = $5e_{Std}$. E) Simulated survival rate as a function of elongational length for different numbers of binding spots $N_{total}$ from r=1000 runs per value of $N_{total}$, and r= 100 runs for $N_{total}$ = 1000 and 5000. F) Simulated survival rate as a function of elongation length for $N_{total}$ = 200 for different values of c.*

### Survival rate for different elongation lengths – Simulation of the protein binding kinetics

Using a Monte Carlo approach, the states of a certain number of binding spots (N = 10 to N = 1000) were simulated under the influence of a force equivalent to the passage of a stenosis. The velocity (Figure 7A) significantly determines the tie-off and tie-on rates $k_{on,0}$ and $k_{off,0}$, compare Figure 7B. An example of r = 100 runs with N = 200 binding spots is shown in Figure 7C. We see the number of binding spots in the bound state $N_{on}$ as a function of time. From

these simulations, similar to the analysis of the experiments, a survival rate $s_{sim}$ is determined (compare Figure 7D and equation 9). We compare the survival rate $s_{sim}$ from simulating the protein binding kinetics with the experimental survival rate $s_{exp}$ from Figure 4.

First, results of different variants of the simulation are presented. With the parameters $v_0$ = 0.01 m/s, Δt = 10 µs, $k_{on,0}$ = 1000 and $k_{off,0}$ = 200, the survival rate is obtained as a function of the elongation length as shown in Figure 7E and F. The progression is strongly related to the number of binding spots chosen for the simulation and the factor *c* used to calculate the rate according to equation 9. According to the estimation in equation 8, *c* = 130 was used. The transition length, at which a survival rate of 50% is achieved, shifts to smaller values with increasing factor *c*, see Figure 7F. For different number of binding spots, the transition length is constant, but the curve becomes significantly steeper with increasing number , see Figure 7E. After comparison with Figure 4A, the curve for *c* = 130 and $N_{total}$ = 200 binding spots, respectively, corresponds most closely to the experimental results of rosettes. In addition, the value of the transition length with $e \approx 1.25 e_{Std} = 69\mu\mathrm{m}$ is in the range of the transition lengths of 50–100 µm determined in the experiment, see Figure 4B.

The reduction of the absolute values of $k_{on,0}$ and $k_{off,0}$ at the same ratio essentially preserves position and shape of the step in s(e). While reducing the tie-on and tie-off rates for constant $k_{on,0}$/ $k_{off,0}$ results in the same equilibrium number of bound proteins, the dynamics are different. Here, especially the return to equilibrium after passing the stenosis runs slower with lower absolute values of $k_{on,0}$ and $k_{off,0}$. In order to keep the process out of a deterministic regime, $P = k\Delta t$ must remain significantly smaller than 1. A capping of the rate with $P_{max}$ = 0.5 has no influence on the results, even with $P_{max}$ = 0.1 the difference is small or leads to higher survival rates only for short elongation lengths. Shortening of the time steps to one tenth resulted in identical curves (results not shown here).

Based on the experimentally determined results presented in Figure 3 and 4 we adjusted the original hypothesis as follows. We assume that the increased exposure time (in the range of 5-10 ms) that comes with an increased elongation length contributes stronger to rosette disruption than the decreased elongation rate reduces the probability for rosette disruption. Summarizing the Monte Carlo simulations, we obtained the same qualitative and quantitative trends for the survival rate as in the experiments. The best agreement was obtained for $N_{total}$ = 200. Thus, these simulation results are in line with our adapted hypothesis.

## CONCLUSION

In this study, the stability of malaria infected red blood cell aggregates, so called rosettes, during passage of stenoses with different elongation lengths and thus different times of exposure to elongation forces acting on the cell aggregates was investigated. Rosettes were tracked along the channel and categorized into the three states “undamaged”, “damaged” and “totally disrupted” after passage of a stenosis. We define the survival rate as the sum of the undamaged and damaged proportions. The focus was to elucidate the influence of the rosette size, blood group and geometry of the stenosis on the survival rate. Classification by size allowed us to highlight the differences in binding strength between blood groups 0 and A.

The key findings are that larger rosettes, which can afford losing more cells before being considered disrupted, tend to be more durable. Second, a longer stenosis leads to more frequent disruption of the rosettes, implying that not higher elongational rates but longer

exposure to elevated shear and elongational flow is critical. Model systems in experiment and simulation support these observations. To differentiate the impacts of elongational rate, exposure time and stenosis length in the future, a respective set of microchannels could be designed to vary each parameter individually.

Our findings are important as they identify mechanisms leading to aggregate disruption, which expose malaria-infected cells. Exposed malaria-infected cells are more accessible and easier to be cleared by the immune system. It would be fascinating to investigate the disruption dynamics of rosettes *in vivo*.

## AUTHOR CONTRIBUTIONS.

Conceptualization: A.M.J., M.W., T.K. and C.W.; Investigation: A.M.J., A.S., A.M., K.M., T.K. and C.W., Methodology: K.M & A.M.J., Software: A.M.J., Data curation, formal analysis and validation: A.M.J., A.S., A.M., K.M., T.K. and C.W., Supervision and resources: M.W., T.K. and C.W., Writing-original draft: A.M.J., T.K. and C.W., Writing – review & editing: A.M.J., A.S., A.M., K.M., M.W., T.K. and C.W..

## DECLARATION OF INTERESTS.

The authors declare no competing interests.

## ACKNOWLEDGEMENT

A.M.J. and C.W. would like to acknowledge funding by Nanosystems Initiative Munich (NIM), the Center for NanoScience (CeNS), the “Studienstiftung des deutschen Volkes,” and the “Programm für Chancengleichheit” of the University of Augsburg for financial support, allowing for, among others, several research stays at the Karolinska Institute. C.W. would like to acknowledge funding by the DFG (INST 94/135-1 FUGG, 508235635). Moreover, we thank Dr. Gerhard Schmid for fruitful discussions.

LITERATURE


1. Moll K, Palmkvist M, Ch'ng J, Kiwuwa MS, Wahlgren M. Evasion of Immunity to Plasmodium falciparum: Rosettes of Blood Group A Impair Recognition of PfEMP1. Braga ÉM, editor. PLoS One. 2015 Dec;10(12):e0145120.
2. Paing MM, Salinas ND, Adams Y, Oksman A, Jensen ATR, Goldberg DE, et al. Shed EBA-175 mediates red blood cell clustering that enhances malaria parasite growth and enables immune evasion. Elife. 2018;7:1–18.
3. Vahidi B, Fatouraee N. Large deforming buoyant embolus passing through a stenotic common carotid artery: A computational simulation. J Biomech. 2012;45(7):1312–22.
4. Musoke C, Ssendikadiwa C, Babua C, Schwartz J. Severe falciparum malaria associated with massive pulmonary embolism. Ann Afr Med. 2014;13(1):47–9.
5. Okeniyi J, Kuti B. Cerebral Malaria in Children with Cyanotic Heart Diseases - The Need for a Closer Look. Congenital Heart Disease 3.1; 2008.
6. McQuaid F, Rowe JA. Rosetting revisited: A critical look at the evidence for host erythrocyte receptors in Plasmodium falciparum rosetting. Parasitology. 2020;147(1):1–11.
7. Nash GB, Cooke BM, Carlson J, Wahlgren M. Rheological properties of rosettes formed by red blood cells parasitized by Plasmodium falciparum. Br J Haematol. 1992;82(4):757–63.
8. Chu Y, Haigh T, Nash G. Rheological analysis of the formation of rosettes by red blood cells parasitized by Plasmodium falciparum. Br J Haematol [Internet]. 1997 [cited 2015 Jun 8];777–83. Available from: http://onlinelibrary.wiley.com/doi/10.1046/j.1365-2141.1997.4643268.x/full
9. Adams Y, Rowe JA. The effect of anti-rosetting agents against malaria parasites under physiological flow conditions. PLoS One [Internet]. 2013 Jan [cited 2015 Jun 8];8(9):e73999. Available from: http://www.pubmedcentral.nih.gov/articlerender.fcgi?artid=3774797&tool=pmcentrez&rendertype=abstract
10. Jötten AM, Moll K, Wahlgren M, Wixforth A, Westerhausen C. Blood group and size dependent stability of P. falciparum infected red blood cell aggregates in capillaries. Biomicrofluidics [Internet]. 2020 Mar;14(2):024104. Available from: http://aip.scitation.org/doi/10.1063/1.5125038
11. Cserti CM, Dzik WH. Review article The ABO blood group system and Plasmodium falciparum malaria. Blood. 2007;110(7):2250–8.
12. Rowe JA, Handel IG, Thera MA, Deans A, Lyke KE, Koné A, et al. Blood group O protects against severe Plasmodium falciparum malaria through the mechanism of reduced rosetting. Proc Natl Acad Sci U S A [Internet]. 2007 Oct 30 [cited 2015 Jun 8];104(44):17471–6. Available from: http://www.pubmedcentral.nih.gov/articlerender.fcgi?artid=2077280&tool=pmcentrez&rendertype=abstract
13. Fry AE, Griffiths MJ, Auburn S, Diakite M, Forton JT, Green A, et al. Common variation in the ABO glycosyltransferase is associated with susceptibility to severe Plasmodium falciparum malaria. Hum Mol Genet. 2008;17(4):567–76.

14. Theron M, Cross N, Cawkill P, Bustamante LY, Rayner JC. An in vitro erythrocyte preference assay reveals that Plasmodium falciparum parasites prefer Type O over Type A erythrocytes. Sci Rep. 2018;8(1):1–9.

15. Sing CE, Alexander-Katz A. Elongational Flow Induces the Unfolding of von Willebrand Factor at Physiological Flow Rates. Biophys J [Internet]. 2010 May;98(9):L35–7. Available from: http://dx.doi.org/10.1016/j.bpj.2010.01.032

16. Moll K, Ljungström I, Perlmann H, Scherf A, Wahlgren M. Methods in Malaria Research. Evaluation. 2008;1-3,17-21.

17. Xia Y, Whitesides GM. Soft Lithography. Annu Rev Mater Sci. 1998;28(1):153–84.

18. Jötten AM. SURF Survival of Rosettes in Flow. 2021.

19. Zhu C. Kinetics and mechanics of cell adhesion. J Biomech. 2000;33(1):23–33.

20. Rakshit S, Sivasankar S. Biomechanics of cell adhesion: How force regulates the lifetime of adhesive bonds at the single molecule level. Phys Chem Chem Phys. 2014;16(6):2211–23.

21. Quadt KA, Barfod L, Andersen D, Bruun J, Gyan B, Hassenkam T, et al. The Density of Knobs on Plasmodium falciparum-Infected Erythrocytes Depends on Developmental Age and Varies among Isolates. PLoS One. 2012;7(9):1–8.

22. Bell GI. Models for the specific adhesion of cells to cells. Science (80- ). 1978;200(4342):618–27.

23. Scherer POJ, Fischer SF. Kramers Theory. In: Theoretical Molecular Biophysics. Berlin, Heidelberg: Springer Berlin Heidelberg; 2017. p. 113–8.

24. Armistead FJ, Gala De Pablo J, Gadêlha H, Peyman SA, Evans SD. Cells Under Stress: An Inertial-Shear Microfluidic Determination of Cell Behavior. Biophys J [Internet]. 2019 Mar;116(6):1127–35. Available from: https://linkinghub.elsevier.com/retrieve/pii/S0006349519301043

25. Carlson J. Plasmodium falciparum erythrocyte rosetting is mediated by promiscuous lectin-like interactions. J Exp Med. 1992;176(5):1311–7.